Available online at www.sciencedirect.com
ScienceDirect
Journal of Sound and Vibration 304 (2007) 50–71
JOURNAL OF SOUND AND VIBRATION
www.elsevier.com/locate/jsvi

Nonlinear biodynamics of passengers coupled with quarter car models

C. Papalukopoulos, S. Natsiavas*

Department of Mechanical Engineering, Aristotle University, 54 124 Thessaloniki, Greece

Received 15 July 2005; received in revised form 10 January 2007; accepted 23 January 2007

Abstract

Biodynamic response of lumped parameter passenger-seat models coupled with simplified models of ground vehicles is investigated. The relatively small dimension of the resulting mechanical models is counterweighted by the complexity introduced by the strongly nonlinear characteristics exhibited by the components of both the biodynamic and the car subsystems. This complexity is enhanced further by the possibility of loss of contact allowed to take place between the wheel and the ground or the passenger and the seat, during strong excitation. After setting up the equations of motion, appropriate methodologies are developed, capturing the dynamic response of the coupled system to transient, harmonic and stochastic excitation, caused by road irregularities. Then, numerical results are presented, illustrating the effect of the excitation amplitude and frequency content on several response quantities related to the dynamic performance of the human and the vehicle components. Special emphasis is put on examining the influence of the seat suspension stiffness and damping characteristics. The results indicate that the nonlinear properties of the coupled model affect significantly its dynamics and can lead to large quantitative and qualitative deviations from the predictions of the corresponding linearized models. Among other things, complex motions are captured, even for harmonic excitation, when the forcing frequency lies between neighboring natural frequencies of the linearized system.

1. Introduction

The systematic and reliable determination of ride comfort and safety of vehicle drivers and passengers is a diverse, multidisciplinary and challenging subject, which has become an issue with a large scientific (bioengineering) component and many important design, commercial and legal aspects. First, it is commonly understood and accepted that human response to dynamic excitation depends on many mechanical, physical, physiological and psychological parameters [1–3]. As a consequence, in addition to performing analytical or numerical studies, a good understanding of the relation between exposure to whole-body human vibration and comfort requires extensive laboratory and real environment experimental studies on the response of the human body to single or multifrequency deterministic excitation or appropriately selected random forcing.

*Corresponding author. Tel.: +30 2310 99 6088; fax: +30 2310 99 6029.
E-mail address: natsiava@auth.gr (S. Natsiavas).

0022-460X/$ - see front matter © 2007 Elsevier Ltd. All rights reserved.
doi:10.1016/j.jsv.2007.01.042

Due to its large practical importance, there is a vast literature devoted to the subject. However, most of the previous studies on ride comfort in road vehicles employed either simplified (lumped parameter) or more involved (finite-element) mechanical models of the driver- or the passenger-seat subsystem, without considering the effects from the coupling with the dynamics of the vehicle [4–7]. Moreover, most of the biodynamic models considered previously possessed linear characteristics, permitting a convenient frequency domain approach, which is compatible with classical experimental procedures [2–7]. On the other hand, preliminary results obtained with both simplified and large-scale finite-element car models have indicated that the coupling between the biodynamic and the car models is important, especially within the critical frequency range 1–10 Hz [8]. In addition, there exists already a substantial part of the literature, referring to previous experimental and numerical studies where the human body nonlinearities are recognized to play a significant and sometimes dominant role in the human dynamics [9–12]. Specifically, careful measurements have indicated a softening effect in the human response through examination of typical parameters, like apparent mass and transmissibility functions. These parameters are defined conveniently within the framework of the linear vibration theory and can be easily obtained experimentally. However, previous analytical and experimental works have also demonstrated that the corresponding response graphs deform and deviate from the predictions of the linear theory as the excitation amplitude increases.

The main objective of the present work is to develop and apply systematic numerical methodologies leading to sufficiently accurate determination of the dynamic response of human models coupled with classical quarter car models, resulting from transient, periodic or stationary random road excitation. Besides the human-structural coupling, the attention is also focussed on examining the effect of both the biodynamic and the car model nonlinearities on the response, as a function of the forcing level caused by the road irregularities, in a numerically effective manner. In this respect, a unique feature of the present work is the modeling of the separation that can occur between the wheel and the ground or between the pelvis and the seat during some intervals of the system response. First, the emphasis is placed on revealing the influence of the excitation amplitude and frequency content on the dynamic response of the coupled system. At the same time, a thorough investigation is performed on the effect of the stiffness and damping parameters of the seat suspension on the human response. The information gathered is useful in predicting the fatigue limits and in assessing potential injury of the passengers, based on various criteria and standards set up by several international committees [1,13,14]. Moreover, the results obtained shed some more light and provide a new and better perspective in interpreting and explaining the outcome of some of the experimental and numerical findings of earlier studies. In addition, they are expected to provide a good foundation for performing more involved studies on the dynamics, identification and optimization of similar and more complex finite-element models of both the vehicle and the human passengers.

The organization of this paper is as follows. First, the necessary theoretical ingredients leading to the equations of motion of the coupled human-seat and vehicle mechanical models are included in the following section. Then, typical numerical results are presented for the response of both the human and the vehicle components. Initially, basic features of the dynamics resulting when the system is subjected to deterministic (transient or periodic) road excitation are investigated. Next, similar results are also obtained for the same models but when subjected to stationary random road excitation. In all cases, the emphasis is put on revealing the influence of parameters related to the car-seat–human coupling and interaction as well as in examining the effect of the excitation level on the activation of the system nonlinearities. Finally, the most important conclusions of this study are summarized in the last section.

2. Mechanical models—equations of motion

In the preliminary design stages, the prediction of the dynamic response as well as of other important aspects of the behavior of ground vehicles, is most commonly carried over by employing the two degree of freedom quarter car model shown in Fig. 1a. This is mostly due to the simplicity of this model and the qualitatively correct information it provides, especially within the low-forcing frequency range required for ride studies [14–17]. On the other hand, when the response of the driver and the passengers is also needed, several simplified lumped parameter models are available, depending on the focus of the study [3–5,11,12]. For the purposes of the present investigation, it was decided to select the discrete model presented in Fig. 1b as the

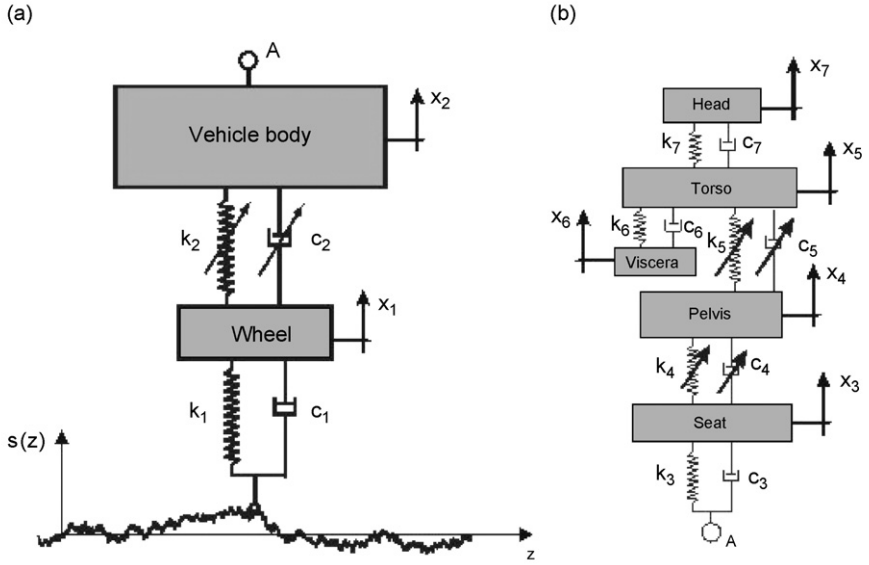

Fig. 1. (a) Quarter car model; (b) biodynamic model.

most appropriate biodynamic model to be coupled with the vehicle model of Fig. 1a, when studying only vertical vibration of the complete system. This was done for two basic reasons. First, besides the seat, this model distinguishes the response of the most important human components, including the pelvis, the upper torso (consisting of the lumbar, thoracic and cervical part of the spine plus the thorax), the viscera (including solid organs like the liver, spleen, pancreas and kidneys as well as hollow organs like the stomach, intestines, urinary bladder and uterus) and the head. In addition, this model is appropriate to capture response of the human, even when the excitation levels are quite high and approach shock loading conditions [11,12].

When both the vehicle and the human models shown in Fig. 1 are assumed to possess linear characteristics, the equations of motion of the resulting coupled model can be put in the classical matrix form

$$\mathbf{M}\ddot{\mathbf{x}} + \mathbf{C}\dot{\mathbf{x}} + \mathbf{K}\mathbf{x} = \mathbf{f}(t), \tag{1}$$

where the quantities **M**, **C** and **K** are the mass matrix, the damping matrix and the stiffness matrix of the dynamical system examined, respectively. Moreover, the vector

$$\mathbf{x}(t) = (x_1 \;\; x_2 \;\; \cdots \;\; x_7)^{\mathrm{T}}$$

includes the displacements of the wheel, the car body, the seat and the four degrees of freedom of the human body. In particular, the dynamic coordinates x_1, x_2 and x_3 represent the absolute vertical displacements of the tire-wheel assembly, the vehicle body and the seat, while the coordinates x_4, x_5, x_6 and x_7 are the displacements of the pelvis, the torso, the viscera and the head, respectively. Finally, the vector $\mathbf{f}(t)$ includes the forcing terms, which can be split in the following form:

$$\mathbf{f}(t) = \mathbf{f}_0 + \mathbf{f}_1(t).$$

More specifically, the constant component of the loading vector has the form

$$\mathbf{f}_0 = -(m_1 g \;\; m_2 g \;\; \cdots \;\; m_7 g)^{\mathrm{T}}$$

and includes the contribution of the gravity loads. On the other hand, the time variant excitation term arises from the road profile geometric irregularities. Namely, if the vehicle travels with a constant horizontal speed v_0 over a road with a profile $s(z)$, this part of the forcing vector is expressed in the form

$$\mathbf{f}_1(t) = (k_1 x_g + c_1 \dot{x}_g \;\; 0 \;\; \cdots \;\; 0)^{\mathrm{T}},$$

where $x_g(t) = s(v_0 t)$. The road elevation profiles selected here are characterized by the existence of either isolated potholes and humps or by continuously distributed surface irregularities.

In many cases, involving relatively high levels of excitation, the linearized version of the equations of motion presented above does not lead to sufficiently accurate results or cannot even predict and explain behavior observed during operation or experimental testing of the system. For such cases, the nonlinearities appearing at both the car and the human-seat model should be taken into account. Then, the equations of motion of the composite system can be put in the form:

$$\mathbf{M}\ddot{\mathbf{x}} + \mathbf{C}\dot{\mathbf{x}} + \mathbf{K}\mathbf{x} + \mathbf{h}(\mathbf{x}, \dot{\mathbf{x}}) = \mathbf{f}(t), \tag{2}$$

where the vector $\mathbf{h}(\mathbf{x}, \dot{\mathbf{x}})$ includes the nonlinear terms arising from the action of the coupled dynamical system examined.

For instance, strongly nonlinear terms are introduced in the equations of motion when the excitation causes the vehicle response to exceed certain limits. In particular, special stoppers are installed in the car suspension unit in order to avoid collisions of the tire-wheel assembly with the vehicle body [17]. As a consequence, the restoring force developed in a typical car suspension can be represented with sufficient accuracy by the following expression:

$$f_s(\delta_2) = \begin{cases} k_{2c}\delta_2 + (k_2 - k_{2c})\delta_{2c} & \text{if } \delta_2 > \delta_{2c}, \\ k_2\delta_2 & \text{if } \delta_{2e} \leqslant \delta_2 \leqslant \delta_{2c}, \\ k_{2e}\delta_2 + (k_2 - k_{2e})\delta_{2e} & \text{if } \delta_2 < \delta_{2e}, \end{cases} \tag{3}$$

where the quantity

$$\delta_2 = x_1 - x_2$$

yields the suspension spring deformation, while δ_{2c} and δ_{2e} represent specific clearance lengths in the suspension. Moreover, the damping force developed in the suspension damper, placed between the car body and the wheel, can be expressed in the form:

$$f_d(\dot{\delta}_2) = \begin{cases} c_{2c}\dot{\delta}_2 & \text{if } \dot{\delta}_2 \geqslant 0, \\ c_{2e}\dot{\delta}_2 & \text{if } \dot{\delta}_2 < 0. \end{cases} \tag{4}$$

This means that the suspension damping coefficient takes a different value in compression than in extension, depending on the sign of the relative velocity between the sprung and the unsprung mass of the car, which is also typical in automotive engineering practice [14,18]. Finally, when the ground is rough, the tire may occasionally separate and lift off the ground temporarily. Specifically, if

$$\delta_1 = x_g - x_1 \quad \text{and} \quad F_1 = k_1\delta_1 + c_1\dot{\delta}_1$$

represent the relative vertical displacement and the force developed between the wheel and the ground, respectively, then the establishment of contact between the wheel and the ground occurs when the kinematical condition

$$\delta_1 = 0$$

is satisfied, while the loss of contact between the wheel and the ground is detected when the kinetic condition

$$F_1 = 0$$

is satisfied [19,20].

On the other hand, many earlier studies have shown that the behavior of the biodynamic model is also characterized by strong nonlinearities. More specifically, adopting the model employed in Refs. [11,12], one of the main nonlinearities appears between the seat and the pelvis. Assuming that the seat cushion stiffness is represented by a linear spring with equivalent stiffness coefficient k_c, which is connected in series with the pelvis spring, the restoring force between the seat and the pelvis is represented by a spring with an equivalent stiffness coefficient:

$$k_4(\delta_4) = \frac{k_p(\delta_{4p})k_c}{k_p(\delta_{4p}) + k_c}.$$

In the last expression, the relative displacement between the seat and the pelvis is defined by

$$\delta_4 = x_3 - x_4$$

and can be split in the form:

$$\delta_4 = \delta_{4c} + \delta_{4p},$$

where δ_{4c} and δ_{4p} correspond to the displacement of the cushion and the pelvis spring, respectively, while

$$k_p(\delta_{4p}) = 1.6215 \times 10^8\, \delta_{4p}^2 \tag{5}$$

represents the equivalent stiffness of the pelvis spring. The model employed takes into account the possibility of loss of contact between the pelvis and the seat, corresponding to a strongly nonlinear dynamic function. Again, the establishment of contact is detected by considering the relative distance between the pelvis and the seat, namely when

$$\delta_4 = 0$$

while a loss of contact between the pelvis and the seat occurs when the kinetic condition

$$F_4 = 0$$

is fulfilled [19,21], where

$$F_4 = k_4(\delta_4)\delta_4 + c_4(\dot{\delta}_4)\dot{\delta}_4$$

is the force developed between the pelvis and the seat.

Likewise, according to information presented in previous studies [11,12], the equivalent stiffness coefficient of the spring connecting the pelvis and the torso is expressed in the form:

$$k_5(\delta_5) = 3.7806 \times 10^6 + 1.09 \times 10^7\, \delta_5 - 2.6868 \times 10^7\, \delta_5^2 \tag{6}$$

with

$$\delta_5 = x_4 - x_5.$$

Moreover, the stiffness nonlinearities arising between the seat and the pelvis as well as between the pelvis and the torso are also transferred to the corresponding damping forces, since the damping coefficients of the biodynamic model are defined by the following relation:

$$c_n(\delta_n) = \zeta_n \sqrt{m_n k_n(\delta_n)} \tag{7}$$

with

$$\delta_6 = x_5 - x_6 \quad \text{and} \quad \delta_7 = x_5 - x_7.$$

Finally, strongly nonlinear terms may also be introduced by the action of the seat suspension system and soft cushion, which however were not considered in the present study.

When the linearized (around the static equilibrium position) equations of motion of the dynamical system examined are considered, there exist standard analytical methodologies that can be employed for capturing its response to both deterministic and stochastic excitation [22]. However, when the excitation levels are such that the system nonlinearities are activated, only numerical treatment of the equations of motion becomes possible [23]. In the following section, characteristic numerical results are presented, which were obtained by considering different types of road excitation.

3. Numerical results

Before presenting results referring to response of the dynamical system examined to road excitation, some useful preliminary information is first in order. With reference to the car model shown in Fig. 1a, the nominal

parameter values are selected to be: $m_1 = 60$, $m_2 = 375\,\text{kg}$, $k_1 = 200$, $k_2 = 15\,\text{kN/m}$, $c_1 = 7$ and $c_2 = 475\,\text{N s/m}$. Moreover, when the suspension possesses bilinear damping, the values of the corresponding damping coefficients in compression and in tension are selected as $c_{2c} = 475$ and $c_{2e} = 1425\,\text{Ns/m}$, respectively. Likewise, the stiffness coefficients of the suspension stoppers are $k_{2c} = k_{2e} = 700\,\text{kN/m}$, with clearance lengths $\delta_{2e} = 0.18\,\text{m}$ and $\delta_{2c} = 0.36\,\text{m}$. On the other hand, the default values for the parameters of the biodynamic model shown in Fig. 1b are chosen as: $m_4 = 29\,\text{kg}$ and $\zeta_4 = 0.25$ for the pelvis, $m_5 = 21.8\,\text{kg}$ and $\zeta_5 = 0.11$ for the upper torso, $m_6 = 6.8\,\text{kg}$, $k_6 = 2831.8\,\text{N/m}$ and $\zeta_6 = 0.5$ for the viscera and $m_7 = 5.5\,\text{kg}$, $k_7 = 202.286\,\text{kN/m}$ and $\zeta_7 = 0.10$ for the head. Finally, the values of the parameters for the seat are selected as $m_3 = 8\,\text{kg}$, $k_3 = 500\,\text{kN/m}$ and $\zeta_3 = 0.5$, while the soft seat cushion has a negligible mass and its action is modeled by a linear spring and damper with stiffness coefficient $k_c = 37.7\,\text{kN/m}$ and damping coefficient $c_c = 159\,\text{Ns/m}$.

The aforementioned values of the car model parameters were employed in previous studies [17,18] and correspond to one quarter of a real car structure [24]. Moreover, the parameters of the biodynamic model employed have been selected based on data obtained from dynamic tensile tests [11,12]. Note that the total mass of the biodynamic model is only about 70% of the passenger mass, since the remaining part is supported by the feet [1].

With the above values for the mass and stiffness parameters, the natural frequencies of the corresponding linearized and undamped car system shown in Fig. 1a are evaluated to be 0.97 and 9.53 Hz, while the associated mode shapes involve large components in the vehicle body and the wheel subsystem, respectively. Likewise, the natural frequencies of the linearized biodynamic model alone are: 3.11, 5.05, 31.86, 42.08 and 88.72 Hz, while the natural frequencies of the linearized coupled system are found to be: 0.89, 3.17, 5.36, 9.53, 31.86, 42.44 and 88.72 Hz. In this way, it becomes obvious that three of the frequencies of the coupled model are identical to frequencies of the uncoupled models, for the accuracy level considered. This indicates a weak linear coupling due to large differences in the mass values of the model components.

In order to get an idea of how the seat suspension stiffness coefficient affects the system resonances, Fig. 2a depicts the natural frequencies of the linearized system determined as a function of k_3, over a relatively wide range. The results indicate that an increase in the value of k_3 causes an increase in most of the natural frequencies, over a part of the range of k_3 examined. Obviously, the two modes dominated by the motion of the wheel and the vehicle body are not affected significantly. Likewise, Fig. 2b presents similar results, obtained by fixing k_3 to its default value and by varying the seat cushion stiffness coefficient k_c. The results depicted in Fig. 2b illustrate that the seat cushion flexibility affects mostly two of the lowest three natural frequencies, corresponding to mode shapes which involve a large contribution from the viscera and the pelvis motion. Again, the two modes dominated by the motion of the wheel and the vehicle body are virtually unaffected.

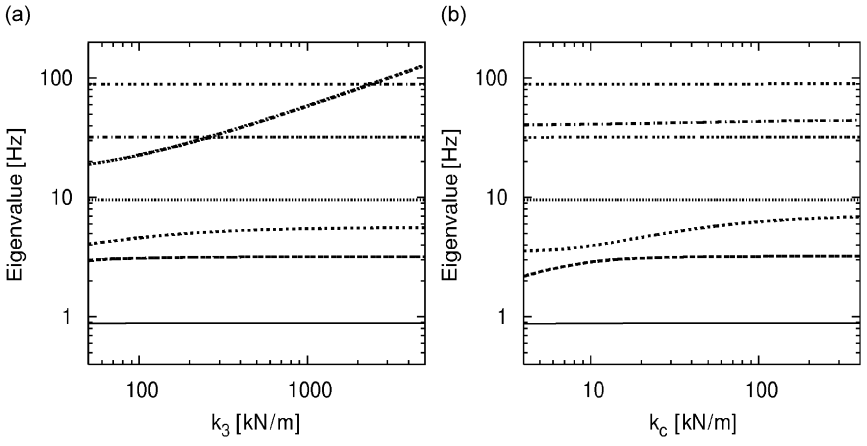

Fig. 2. Dependence of natural frequencies of the linearized coupled system on: (a) the seat suspension stiffness coefficient and (b) the seat cushion stiffness coefficient.

3.1. Results for transient road excitation

In this subsection, typical numerical results are presented, obtained by assuming that the vehicle models examined pass with a constant horizontal speed v_0 over an isolated road irregularity. Among all the possible choices that are available, one of the most characteristic types of irregularities corresponds to a road with a harmonic profile of the form:

$$s(z) = \hat{x}_g \sin(\pi z/\ell) \quad \text{for } 0 \leqslant z \leqslant \ell,$$

where ℓ is the length of the road irregularity. This induces a base excitation on the wheel of the car, with the form:

$$x_g(t) = \hat{x}_g \sin(\omega t + \varphi) \quad \text{for } 0 \leqslant t \leqslant \tau, \tag{8}$$

where φ is an arbitrary phase angle, while the parameters

$$\omega = \frac{\pi v_0}{\ell} \quad \text{and} \quad \tau = \frac{\ell}{v_0}$$

correspond to the forcing frequency and the time it takes for the vehicle to run over the irregularity, respectively. All the results presented in this subsection refer to important aspects and illustrate the dynamics of the systems considered to the imposed excitation.

First, Fig. 3 presents the initial part of the history obtained for some selected response components of the car and the biodynamic model by employing the nominal system parameters, a road profile with $\hat{x}_g = 0.02\,\text{m}$ and $\varphi = 0$ (representing a road with a bump) and four characteristic values of the forcing frequency ω. For convenience, the histories obtained are shown as a function of the normalized time t/τ, so that the time τ is used as a characteristic time. In particular, the results presented in Figs. 3a–d depict the acceleration histories obtained at the four human components of the biodynamic model employed. These quantities are necessary in assessing the fatigue limits or the potential of injury of the passengers. As a first observation, the maximum amplitudes of acceleration determined for each forcing frequency are comparable in all four human components. Moreover, as the forcing frequency increases, this maximum amplitude increases originally and then decreases.

On the other hand, Figs. 3e–h present the same part of the history determined for other selected response quantities, like the wheel acceleration $\ddot{x}_1$, the relative deflection of the suspension spring δ_2, the force F_1 developed between the wheel and the ground and the force F_4 acting between the pelvis and the seat. These quantities are useful in interpreting and explaining the dynamic behavior of the coupled system examined. For instance, direct comparison of the results presented in Figs. 3a–d with those of Fig. 3e illustrates that the car and the seat suspension are proved to be very effective in reducing the acceleration levels transmitted from the road to the passenger. In addition, the results of Fig. 3f demonstrate that the car suspension spring remains in the linear regime for all the forcing frequencies considered. Finally, the results of Figs. 3g and h indicate that there is no time interval where separation is observed to take place between the wheel and the ground (with the exception of a tiny time interval for $\omega = 10\,\text{Hz}$) or the pelvis and the seat, for the excitation level chosen.

The picture changes rapidly when the amplitude of the road hump is increased to $\hat{x}_g = 0.10\,\text{m}$, due to activation of the system nonlinearities. This is illustrated in Fig. 4, which includes exactly the same set of diagrams with Fig. 3. First, comparison of the first five diagrams of these figures demonstrates that there appears a nonproportional increase in the amplitudes of the response acceleration signals. However, even more interestingly, such large levels of excitation are responsible for the appearance of other phenomena, leading to significant qualitative differences in the response. Specifically, the most important information is related to the temporary loss of contact taking place between the wheel and the ground (when $F_1 = 0$) for the cases with $\omega = 5$, 10 and 20 Hz, as can be detected from Fig. 4g. Moreover, the results of Fig. 4h verify a temporary loss of contact occurring between the pelvis and the seat (when $F_4 = 0$) for $\omega = 5$ and 10 Hz. In addition, the large-amplitude oscillation produced causes activation of the compression stoppers in the car suspension spring (when $\delta_2 > \delta_{2c} = 36\,\text{cm}$), for all the excitation frequencies considered, as demonstrated by the results of Fig. 4f.

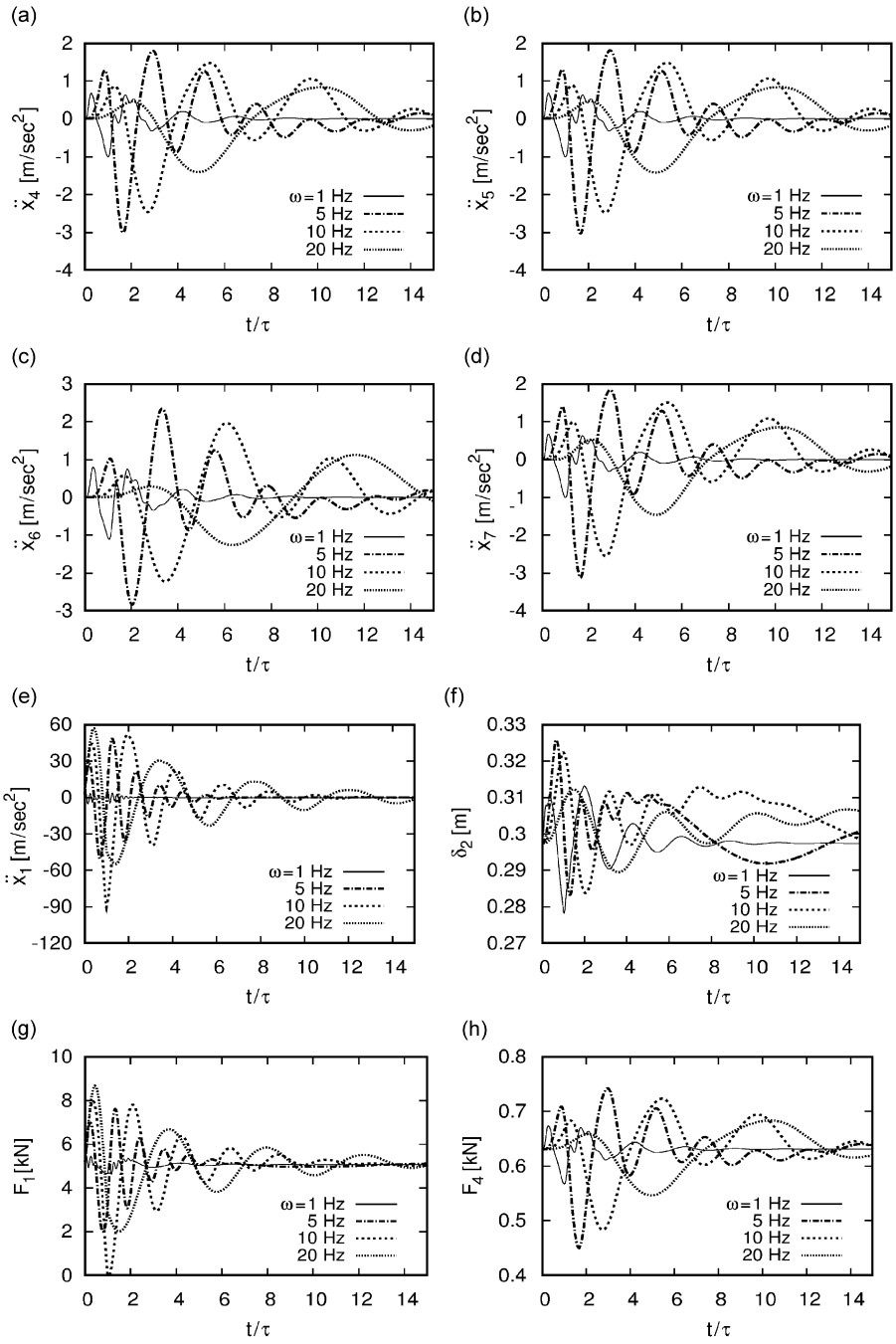

Fig. 3. Acceleration histories obtained at the: (a) pelvis; (b) upper torso; (c) viscera; (d) head and (e) wheel. (f) Relative deflection of the suspension spring; (g) force developed between the wheel and the ground and (h) force between the pelvis and the seat, for a ground profile with $\hat{x}_g = 0.02\,\mathrm{m}$.

The phenomena associated with the activation of the system nonlinearities are intensified further by increasing the road bump amplitude. When this amplitude is high enough, the excitation approaches levels of shock loading. For instance, the continuous lines of Fig. 5 present the histories obtained for the pelvis acceleration, the deformation of the car suspension spring, the force developed between the wheel and the ground and the force between the pelvis and the seat, for $\hat{x}_g = 0.14\,\mathrm{m}$, $\omega = 10\,\mathrm{Hz}$ and $\varphi = 0$. For comparison

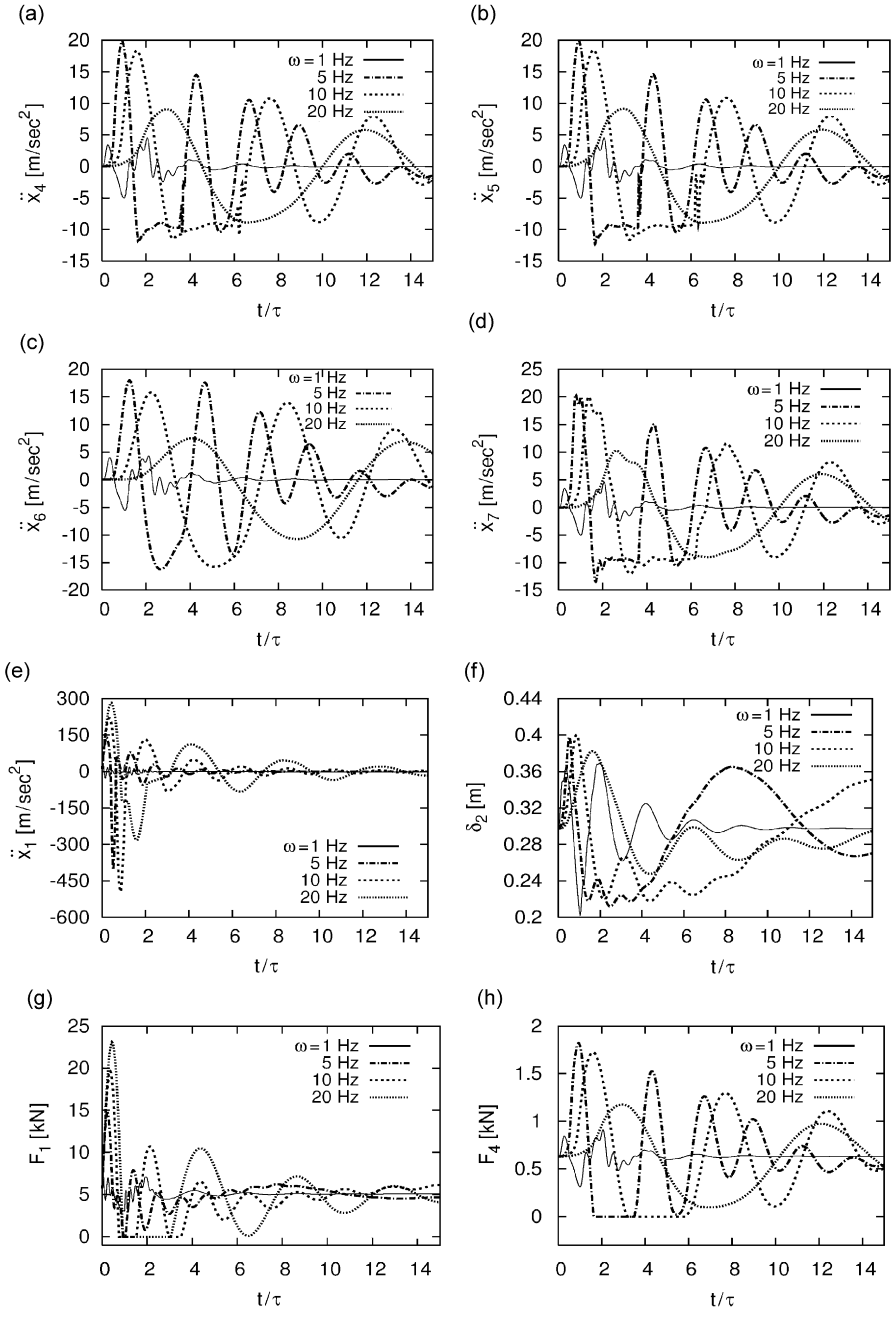

Fig. 4. Acceleration histories obtained at the: (a) pelvis; (b) upper torso; (c) viscera; (d) head and (e) wheel. (f) Relative deflection of the suspension spring; (g) force developed between the wheel and the ground and (h) force between the pelvis and the seat, for a ground profile with $\hat{x}_g = 0.10\,\mathrm{m}$.

purposes, the thin continuous lines represent results determined for the corresponding linearized system. Obviously, large deviations are observed in the predictions of the nonlinear and the linearized model, indicating the importance of including the nonlinear characteristics in the equations of motion. Finally, the other two sets of curves of Fig. 5, represented by broken lines, were captured for $\varphi = \pi$, instead, corresponding to a road with a pothole. Again, the thin broken lines represent results obtained by employing the linearized system. Here, the differences observed are still noticeable but they are not as substantial as they

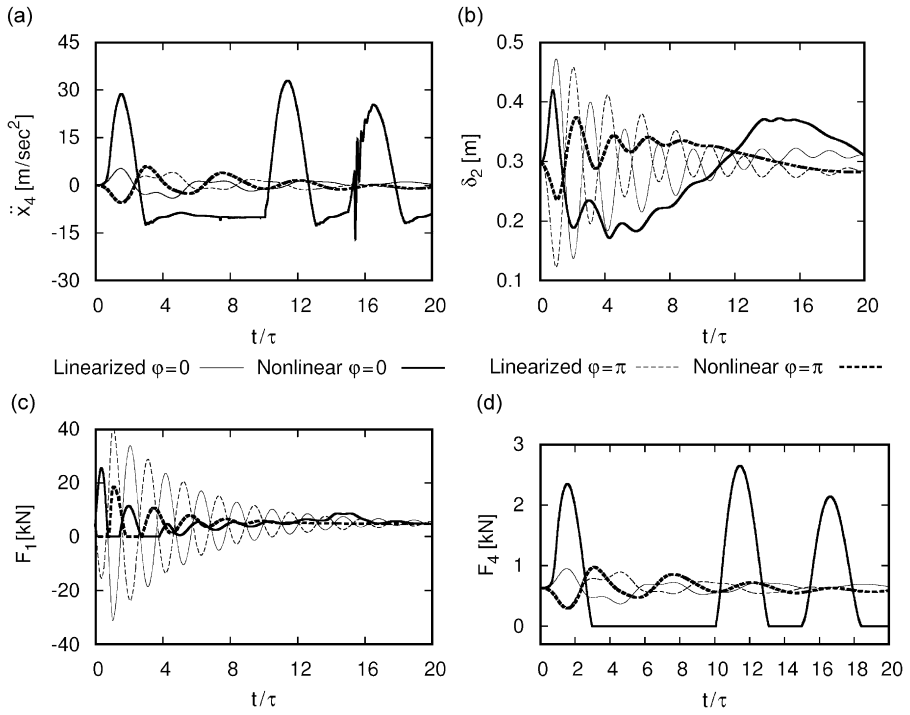

Fig. 5. Histories obtained at $\omega = 10\,\text{Hz}$ and $\hat{x}_g = 0.14\,\text{m}$ for the: (a) pelvis acceleration; (b) deformation of the car suspension spring; (c) force between the wheel and the ground and (d) force between the pelvis and the seat.

were found to be for the case with $\varphi = 0$. This signals a significant effect of the phase on the system response and can be justified by the asymmetry present in the system technical characteristics.

The dynamical system developed and examined in the present study involves several sources of nonlinearities. In an effort to isolate the effects arising from the biodynamic model nonlinearities from the effects caused by the other nonlinearities of the composite model considered, a sequence of diagrams is presented in Fig. 6. In particular, the continuous thin lines of these diagrams represent results obtained after linearizing the stiffness forces of the biodynamic model, expressed by relations (5) and (6), together with the corresponding damping terms. For comparison, the nearby broken curves represent results taken from the previous figure, obtained for the fully nonlinear model with $\hat{x}_g = 0.14\,\text{m}$, $\omega = 10\,\text{Hz}$ and $\varphi = 0$, which is the case involving the largest activation level of the nonlinearities. Clearly, the results demonstrate that the effect of the biodynamic model nonlinearities alone is quite small, even for this relatively high level of excitation. In fact, the results obtained from these two different models for smaller values of $\hat{x}_g$ were practically indistinguishable. On the other hand, observable deviations started appearing for much larger values of $\hat{x}_g$. This means that most of the nonlinear action arising at the excitation levels considered is due to the nonlinearities of the structural part of the system examined, including the loss of contact. Moreover, the nonlinearities of the biodynamic model are activated and become important for very high excitation levels only, as expected [11,12].

Among all the structural components, the seat is expected to have a large influence on the human response, since it is in direct contact with the passenger. The following sequence of diagrams illustrates the effect of the seat suspension stiffness and damping coefficients on the response of the biodynamic model. Among other things, such information is useful in the efforts to optimally select the seat suspension stiffness and damping properties. First, Fig. 7 presents results obtained for a road bump with $\hat{x}_g = 0.10\,\text{m}$ and forcing frequency $\omega = 10\,\text{Hz}$, by varying the equivalent stiffness coefficient of the seat suspension. More specifically, the horizontal axis shows the value of the normalized seat suspension stiffness, defined by

$$\kappa_3 = \sqrt{k_3/k_s},$$

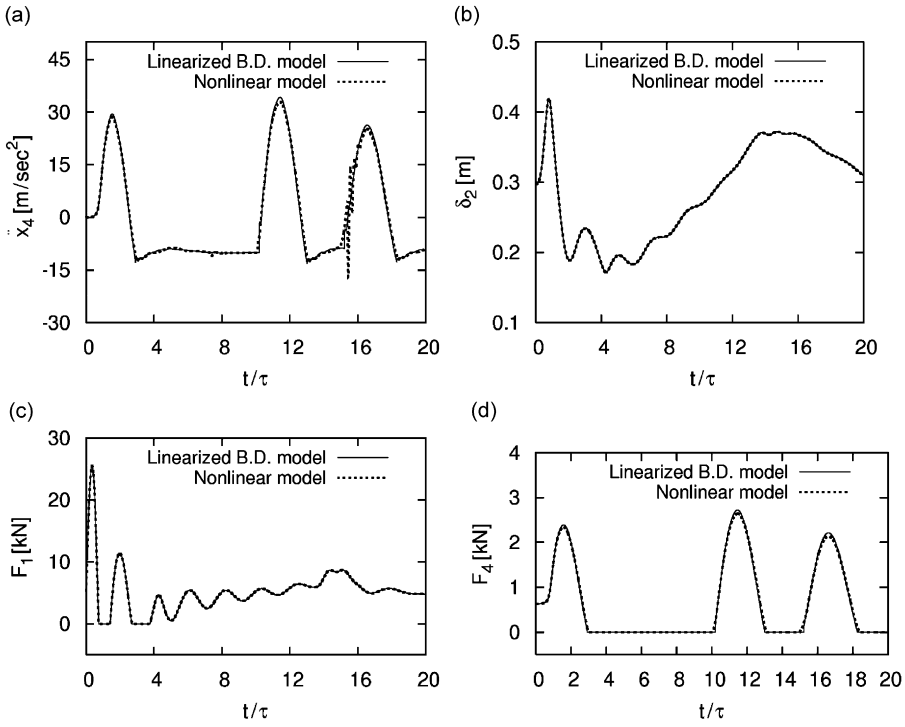

Fig. 6. Histories obtained at $\omega = 10\,\text{Hz}$, $\hat{x}_g = 0.14\,\text{m}$ and $\varphi = 0$ for the: (a) pelvis acceleration; (b) deformation of the car suspension spring; (c) force between the wheel and the ground and (d) force between the pelvis and the seat.

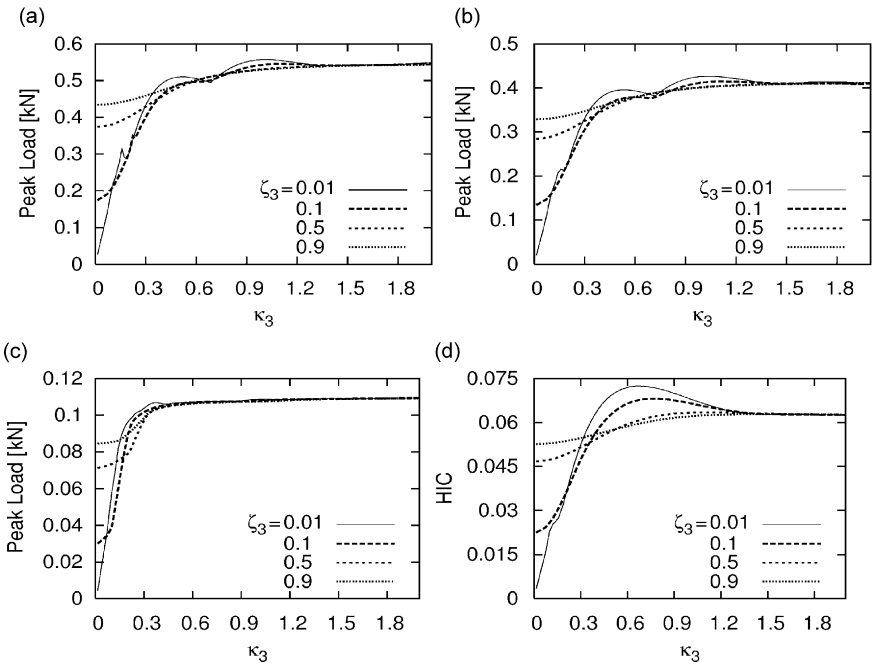

Fig. 7. Peak load for the: (a) pelvis; (b) torso and (c) viscera and (d) head injury criterion, as a function of the normalized seat stiffness κ_3, at $\omega = 10\,\text{Hz}$.

where k_s takes the default value 500 kN/m of the seat suspension stiffness coefficient, while the vertical axis shows the corresponding peak load. This last quantity is defined as the product of the mass times the maximum value of the acceleration history obtained in each forcing case and is evaluated separately for the pelvis, the torso and the viscera. On the other hand, the response of the head is characterized in a better way by the so-called Head Injury Criterion, defined as follows:

$$\mathrm{HIC} = \max\left\{(t_2 - t_1)\left[\frac{1}{(t_2 - t_1)g}\int_{t_1}^{t_2} \ddot{x}_7(t)\,\mathrm{d}t\right]^{2.5}\right\}, \tag{9}$$

where t_1 and t_2 are any two points of the corresponding acceleration history. To prevent evaluation of unrealistically high values of this quantity, it is commonly accepted that $t_2 - t_1 = 15$ ms [11,12].

The numerical results presented in Fig. 7 were evaluated for four widely different values of the seat suspension damping ratio ζ_3. These results indicate that both the seat stiffness and damping properties affect the value of the peak loads and the HIC for relatively small values of the normalized seat suspension stiffness only. After a critical value of κ_3, the effect of varying the seat suspension properties is negligible for all practical purposes. For comparison, Fig. 8 presents similar results, obtained instead for $\omega = 1$ Hz. Among other things, the values presented in Figs. 7 and 8 are useful for injury assessment. However, it should be mentioned that the values determined in the cases examined here are quite small, when compared with the corresponding critical values [11,12].

Finally, Fig. 9 presents similar results, obtained for $\hat{x}_g = 0.10$ m and $\omega = 10$ Hz, as a function of the seat suspension damping ratio ζ_3. In particular, these results were obtained for three characteristic values of the normalized seat suspension stiffness parameter κ_3, covering a relatively wide range of values, according to the results shown in Fig. 7. Once again, the results indicate that the values of both the peak loads and the HIC are more sensitive for relatively small values of the seat suspension stiffness and damping parameters. Overall, the results presented in the last three figures create a sufficiently clear picture of the effects caused by the seat suspension technical parameters on the dynamic response of the coupled system considered.

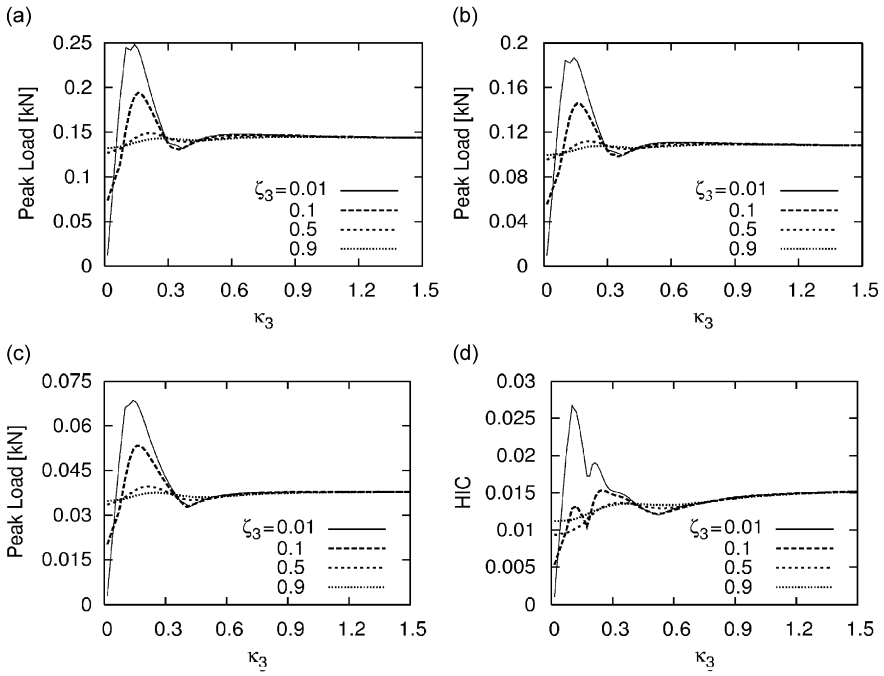

Fig. 8. Peak load for the: (a) pelvis; (b) torso and (c) viscera and (d) head injury criterion, as a function of the normalized seat stiffness κ_3, at $\omega = 1$ Hz.

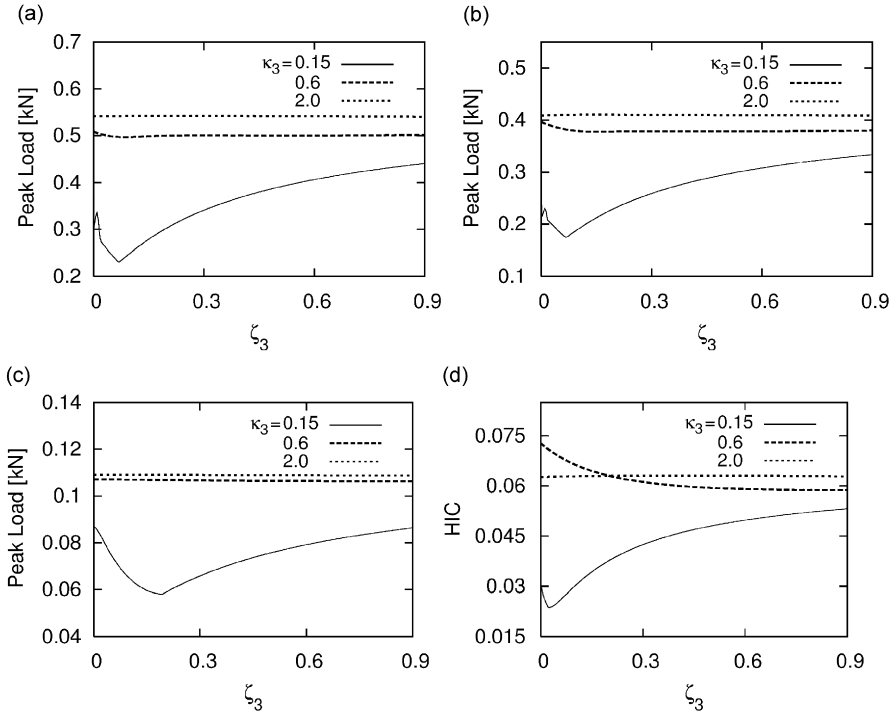

Fig. 9. Peak load for the: (a) pelvis; (b) torso and (c) viscera and (d) head injury criterion, as a function of the seat suspension damping ratio ζ_3, for $\hat{x}_g = 0.10\,\text{m}$ and $\omega = 10\,\text{Hz}$.

3.2. Results for harmonic road excitation

This section presents a sequence of diagrams with characteristic numerical results obtained by assuming that the coupled passenger-seat-vehicle model examined travels with a constant horizontal speed v_0 over a road with harmonic profile, having amplitude $\hat{x}_g$ and wavelength λ. Consequently, the forcing vector $\mathbf{f}_1(t)$ included in the equations of motion (2) is proportional to the road profile amplitude $\hat{x}_g$ and involves harmonic terms with frequency $\omega = 2\pi v_0/\lambda$. In such cases, since the forcing is periodic, that is

$$\mathbf{f}(t + T_E) = \mathbf{f}(t) \quad \text{with} \quad T_E = \lambda/v_0,$$

it is reasonable to expect that the long-term response of the system will also reach a periodic steady state, satisfying the conditions

$$\mathbf{x}(t + T) = \mathbf{x}(t) \quad \text{and} \quad \dot{\mathbf{x}}(t + T) = \dot{\mathbf{x}}(t).$$

The period T of the response is in general a commensurate multiple of the forcing period T_E, with the most common case being $T = nT_E$, corresponding to harmonic ($n = 1$) or subharmonic ($n = 2,3,\ldots$) response. For systems with smooth nonlinear characteristics, proper continuation techniques have been developed in order to locate branches of periodic motions of periodically excited mechanical system, as the fundamental forcing frequency varies [23]. Moreover, suitable methodologies have also been developed for investigating the stability properties of each located periodic motion. However, the discontinuities appearing in the equations of motion of the coupled system examined do not permit direct application of such methodologies [19,21,25]. For this reason, determination of periodic steady-state response of the dynamical systems examined is performed by direct integration of the equations of motion until the transient part of the response dies out. More specifically, branches of stable motions are obtained in this way by applying a sequential continuation method.

The first set of results is presented in the form of typical frequency–response diagrams, obtained for quantities related to the human response for $\kappa_3 = 1$, $\zeta_3 = 0.5$ and several different values of the road profile

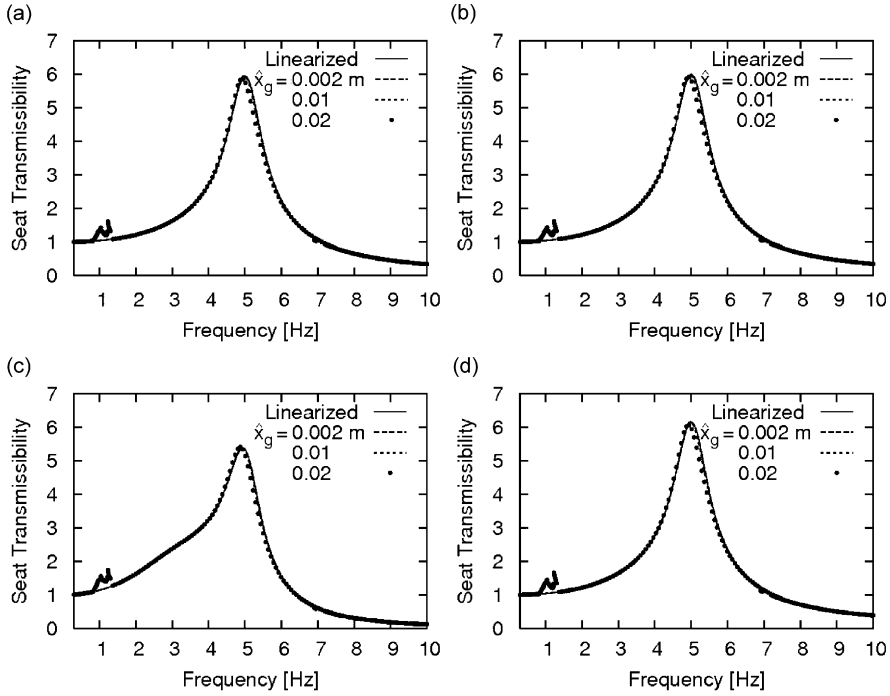

Fig. 10. Seat transmissibility functions of the coupled system for the vertical acceleration at the: (a) pelvis; (b) upper torso; (c) viscera and (d) head.

amplitude. In particular, Fig. 10 depicts the seat transmissibility functions of the biodynamic model components, as a function of the forcing frequency. These quantities are defined as the ratio of the root-mean-square value of the periodic acceleration signal determined for the response quantity examined at each frequency to the corresponding root-mean-square value of the acceleration signal recorded at the seat. As in the case of transient excitation, the values of the functions shown in Fig. 10 for the different degrees of freedom of the biodynamic model are comparable. Moreover, these values are also comparable with similar measured values reported in earlier work [10]. Finally, the nonlinearities affect the results in a significant way, as explained next.

For comparison, the thin curves included in Fig. 10 represent results obtained for the linearized model. Obviously, for small levels of excitation, the transmissibility functions determined for the nonlinear system are virtually identical with those of the linearized system. In fact, in order to achieve this coincidence, the value of the suspension damping coefficients was selected as constant, with $c_2 = 475\,\mathrm{N\,s/m}$. However, as the excitation amplitude increases, some differences start to arise between the predictions of the nonlinear and the linearized coupled models examined. For instance, the main resonance showing off in these diagrams, which appears around 5 Hz and is dominated by the pelvis motion, is shifted to lower frequencies. This is expected for systems possessing asymmetric nonlinear characteristics [23]. Also, a resonance in the vicinity of 1 Hz, which is characterized by large motions of the car and human body, starts becoming more noticeable gradually. More importantly, the branches with periodic steady-state solutions are disconnected at various places, while for sufficiently large excitation amplitudes there appear frequency intervals where no periodic motion is captured. Some of these observations will be investigated in more depth shortly.

Similar conclusions can also be drawn from the results shown in Fig. 11, which depicts the same transmissibility functions, but assuming that the excitation is now applied directly at the base A of the five degrees of freedom biodynamic model shown in Fig. 2a, instead. Comparison with the results depicted in Fig. 10 indicates that the car flexibility effects are important throughout the frequency range examined and make a substantial difference in the frequency range where the resonance of the pelvis occurs. This indicates

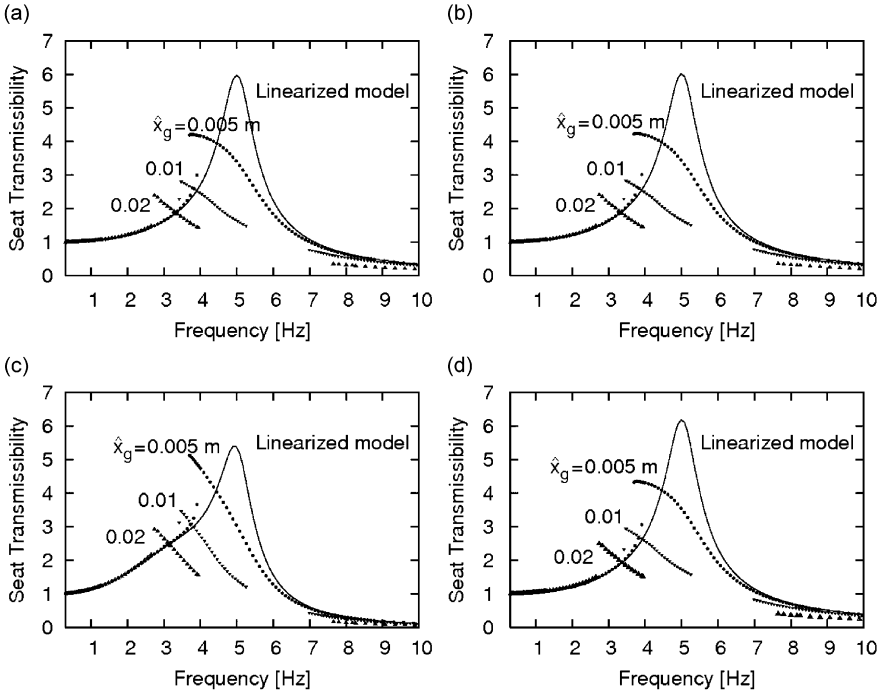

Fig. 11. Seat transmissibility functions of the biodynamic model (shown in Fig. 1b) for the vertical acceleration at the: (a) pelvis; (b) upper torso; (c) viscera and (d) head.

the importance of the coupling between the dynamics of the vehicle and the biodynamic model. Namely, the differences between the results observed in Figs. 10 and 11 illustrate the fact that the vehicle technical characteristics affect significantly the response of the human passengers, especially in the vicinity of frequency ranges corresponding to resonances of the biodynamic model. In particular, the nonlinear behavior of the biodynamic model alone is more clearly manifested in Fig. 11, by a stronger bending of the response curves and by an enlargement of the forcing frequency intervals where no stable periodic steady-state motions can be located. This indicates that the presence of the vehicle component helps in smoothening out the effects caused by the nonlinearity properties of the biodynamic model.

In order to shed more light and gain a better understanding of the results presented so far, Fig. 12 presents the diagram of the root-mean-square value of the acceleration detected at the car wheel and at the pelvis as a function of the forcing frequency, for a similar set of parameters that led to the results shown in Fig. 10. In all cases, the nearby thin lines represent results obtained from the corresponding linearized model. As a general observation, the acceleration levels developed at the wheel are again much higher than those developed at the pelvis, especially within the higher frequency range examined. This demonstrates the effectiveness of the car and seat suspension in isolating the human body from the road excitation. Also, inspection of the diagrams included in Fig. 12a reveals mostly the presence of the resonance dominated by the wheel motion, while the response diagrams in Fig. 12b manifest the presence of the car body and the pelvis resonances, in addition to the wheel resonance.

Once again, the results presented in Fig. 12 illustrate that an increase in the forcing amplitude leads to an increase in the response amplitude and a simultaneous gradual deformation (bending to the left) of the response curves, which is typical of systems with nonlinear and asymmetric restoring forces [23]. As a consequence of this bending, the branches of periodic motions captured appear to be disconnected at some places, which can easily be identified since they are points of vertical tangency and signal the occurrence of saddle-node bifurcations. Besides these points, some solution branches have other missing parts, too, because no (stable) periodic motion could be located within some frequency intervals, even after running the calculations over a relatively large number of forcing periods. This behavior is typical of nonlinear systems

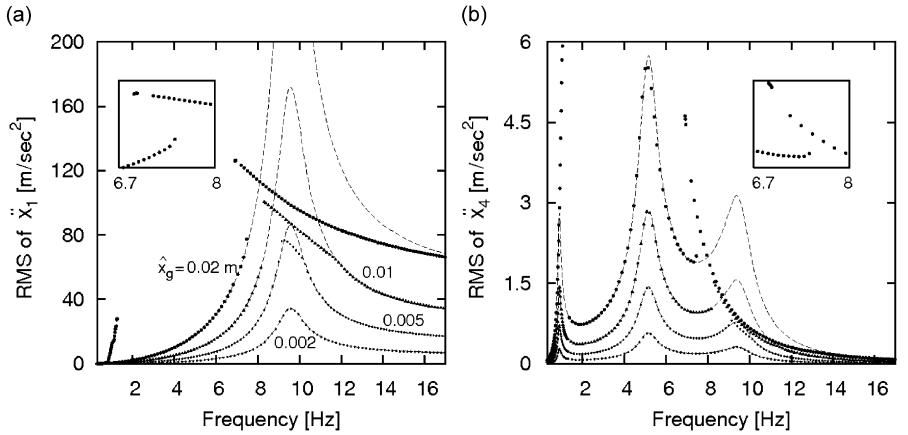

Fig. 12. Root-mean-square value of the acceleration at: (a) the wheel and (b) the pelvis, for several values of the ground profile magnitude $\hat{x}_g$.

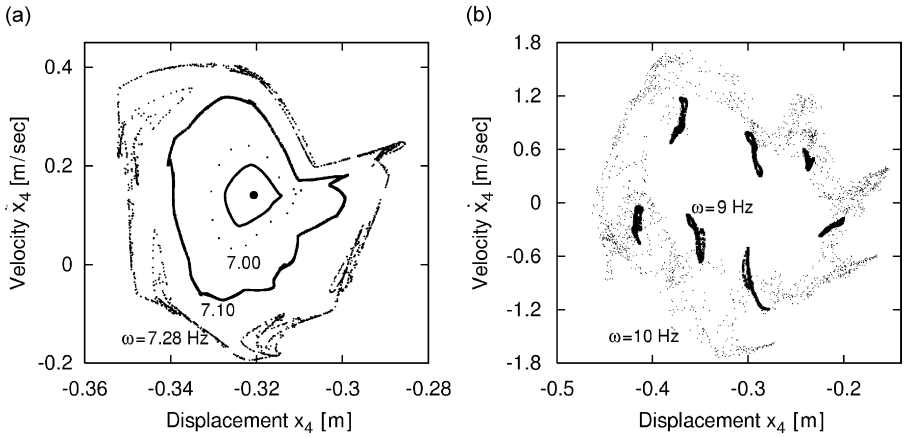

Fig. 13. Poincare sections with the (x_4, $\dot{x}_4$) plane at: (a) $\omega = 6.95$, 6.97, 7.00, 7.10 and 7.28 Hz; (b) $\omega = 9$ and 10 Hz.

and various aspects of it have already been studied extensively in the past [25,26]. Namely, at some critical values of the forcing frequency the periodic motion may lose stability either by a period doubling or by a Hopf bifurcation [27]. For instance, in the specific case with $\hat{x}_g = 0.02$ m, the upper branch of stable periodic motions started from $\omega = 6.91$ Hz, while no periodic motion was located within the frequency range from about $\omega = 6.95$ to 7.17 Hz. This is made more clear by the insets of Fig. 12. This range lies between two neighboring resonances, where the pelvis and the wheel motions dominate the modes of the corresponding linearized system, respectively. In order to explore how is the stability of the periodic motions lost and what is the behavior of the system within that frequency range, a more systematic approach was adopted, leading to the results presented in the following figure.

The results presented in Fig. 13 verify that the loss of stability of the periodic solution at about $\omega = 6.95$ Hz takes place through a Hopf bifurcation. After that frequency, the periodic response gives its place to quasiperiodic motions and culminates eventually into chaotic motions. More specifically, this figure presents the so-called Poincare sections of the trajectories formed in the phase space of the dynamical system examined with the (x_4, $\dot{x}_4$) plane, related to the pelvis degree of freedom. These sections were obtained by integrating the equations of motion of the system for a sufficiently long period of time, so that the original transient response dies out and then plotting one point per forcing period on the (x_4, $\dot{x}_4$) plane. Qualitatively similar results were also derived for sections corresponding to the other degrees of freedom of the model.

The single dot shown in Fig. 13a was obtained at $\omega = 6.95$ Hz and indicates that the motion captured is periodic, with period equal to the forcing period ($n = 1$). Immediately after that frequency value, the single dot gives its place to an invariant circle of dots, representing a motion of the system with modulated amplitude [26]. As the value of the forcing frequency increases further, the size of the attractor formed on the Poincare section increases gradually and may occasionally become locked to a long period subharmonic attractor, like the $n = 17$ attractor obtained at $\omega = 7.00$ Hz. Then, the shape of the attractor starts getting distorted (like the attractor captured at $\omega = 7.10$ Hz) and settles into response characterized by chaotically modulated amplitudes ($\omega = 7.28$ Hz). In fact, further numerical calculations verified that this branch of motions exists up to at least $\omega = 10.45$ Hz and goes through a repetitive sequence of transitions from irregular (chaotic) to regular (long period subharmonic or quasiperiodic) response and vice versa, in accordance with previous theoretical predictions [27]. For instance, Fig. 13b presents the attractors located at $\omega = 9$ and 10 Hz. These attractors are much bigger in size and have more irregular shapes than those included in Fig. 13a.

On the other hand, the upper branch of stable periodic motions terminating at about $\omega = 7.17$ Hz seems to lose stability through a subcritical Hopf bifurcation value, since direct integration of the equations of motion for smaller (but close) values of the forcing frequency leads to either the coexisting lower branch of stable periodic motions shown in Fig. 12 or to the same sequence of amplitude-modulated motions, which are selectively shown in Fig. 13. Taking into account the information presented in the previous paragraph, a possible scenario for the generation, development and extinction of the branch of motions which are similar to those presented in Fig. 13 is the following. Originally, the stable periodic motions belonging to the isolated upper branch of solutions determined for $\hat{x}_g = 0.02$ m lose their stability at about $\omega = 6.95$ Hz via a supercritical Hopf bifurcation. The resulting quasiperiodic or chaotic motions lie on a branch which was found to extend up until $\omega = 10.45$ Hz, where it meets with and annihilates (through a saddle-node bifurcation) a branch of similar but unstable motions. Possibly, this branch of unstable amplitude-modulated motions emanates via a subcritical Hopf bifurcation from the upper branch of the stable periodic motions at about $\omega = 7.17$ Hz. This hysteresis phenomenon has significant practical consequences, which are explained next.

To reveal even more aspects of the complexity associated with the system dynamics over the particular frequency range and combination of parameters examined, it is apparent from the insets of Fig. 12 that there exists a forcing frequency interval where the stable periodic motions lying on the lower branch coexist with the stable periodic motions of the upper branch as well as with the branch of the amplitude-modulated motions. Therefore, taking into account the information presented in the last paragraphs, it becomes clear that the dynamical system considered may reach one or the other of these motions, leading to completely different response, depending solely on the initial conditions. Moreover, based on the comparison between the results shown in Figs. 10 and 11, the nonlinearity effects seem to be even more pronounced when the biodynamic model alone is considered and excited. These features are inherent to the system dynamic behavior and should be taken into account when recording or explaining the outcome of experimental measurements. Since a large portion of the previous studies on the subject and all the current international standards have their foundation on the linear theory, special care should be exercised in treating or explaining data from numerical studies and experimental measurements. Namely, neglecting these characteristics or considering them as anomalies which have to be eliminated or smoothened out through repetition and averaging, as is done for systems with linear characteristics, will contaminate the final results. In fact, this is expected to introduce serious difficulties and mistakes even in the most systematically and carefully designed experiments.

3.3. Results for random road excitation

In the final part of this study, more realistic road profiles were selected. Quite frequently, road profiles leading to a limited bandwidth white noise excitation are chosen [12,22]. Here, a more appropriate colored road excitation was selected. Namely, the vehicle models were assumed to travel over road profiles characterized by real-valued, zero mean, stationary and Gaussian random fields. For their complete statistical description, it is sufficient to specify the power spectral density of the road irregularities, say $S_g(\Omega)$, where $\Omega = 2\pi/\lambda$ is a spatial frequency, corresponding to a harmonic irregularity with wavelength λ. Among the many alternative choices suggested in previous investigations on the subject [28], the geometrical profile of typical

roads is derived from a spectral density function with the following analytical form:

$$S_g(\Omega) = \begin{cases} S_g(\Omega_{\text{ref}})(\Omega/\Omega_{\text{ref}})^{-n_1} & \text{if } \Omega \leqslant \Omega_{\text{ref}}, \\ S_g(\Omega_{\text{ref}})(\Omega/\Omega_{\text{ref}})^{-n_2} & \text{if } \Omega \geqslant \Omega_{\text{ref}}. \end{cases} \tag{10}$$

This has been adopted by the International Organization for Standardization (ISO), where $\Omega_{\text{ref}} = 1/2\pi$ (cycles per meter) is a reference spatial frequency, while the exponents are chosen as $n_1 = 2$ and $n_2 = 1.5$. Moreover, the value of $S_g(\Omega_{\text{ref}})$ provides a measure for the roughness of the road. For the purposes of the present study, several classes of road profiles were selected.

When a linearized model is used, knowledge of the vehicle velocity and the spectral density representing the road profile permits evaluation of the spectral density of the resulting stationary vehicle response through the well-known formula

$$\mathbf{S_{xx}}(\omega) = \mathbf{H}(\omega)\mathbf{S_{gg}}(\omega)\mathbf{H}^{\mathrm{T}*}(\omega). \tag{11}$$

In the last equation, $\omega = \Omega v_0$ is the temporal frequency, the quantities $\mathbf{S_{xx}}(\omega)$ and $\mathbf{S_{gg}}(\omega)$ are the spectral density matrices of the response and the forcing, respectively, while $\mathbf{H}(\omega)$ is the matrix including the frequency response functions of the system [22]. However, the analysis employed for the linearized system is not expected to produce results with acceptable accuracy when the excitation level is such that the system nonlinearities are activated. In these cases, an alternative numerical method can be applied. In brief, using the spectral representation method [17,22], the forcing caused by the road irregularities is approximated by the following finite series:

$$x_g(t) = \sum_{n=1}^{N} s_n \sin(n\omega_0 t + \varphi_n). \tag{12}$$

In the last formula, the amplitudes of the harmonic components are evaluated from the road spectra chosen as

$$s_n = \sqrt{2S_g(n\Omega_0)\,\Delta\Omega},$$

where $\Delta\Omega = \Omega_0 = 2\pi/L$ is the spatial frequency increment and L is the length of the road segment considered. Consequently, selecting the fundamental temporal frequency ω_0 determines the value of the quantity Ω_0 from $\Omega_0 = \omega_0/v_0$, which in turn furnishes the maximum road wavelength. Moreover, the maximum number N of harmonics included in the forcing function (12) is selected based on the maximum excitation frequency desired. For each spectral density of the road profile selected, the response of the system is obtained by integrating the equations of motion for a number of runs, depending on the level of the accuracy level sought. In each run, the corresponding phases φ_n are treated as random variables, following a uniform distribution in the interval $[0,2\pi)$.

First, Fig. 14 presents typical results, obtained for class A (very good quality) road profiles, corresponding to $S_g(\Omega_{\text{ref}}) = 4 \times 10^{-6}\,\text{m}^2/\text{cycle/m}$, according to classification proposed by ISO [1,14,17]. Specifically, Figs. 14a and b show the power spectral density determined for the acceleration of the wheel and the pelvis, respectively, as a function of the forcing frequency and in response to random excitation imposed at the wheels of the vehicle. In all these calculations, the vehicle was assumed to travel with a constant horizontal speed $v_0 = 120\,\text{km/h}$. The results represented by the continuous and the broken curves were obtained by applying the spectral representation method and averaging the output over a number of runs. In particular, the statistical averaging needed in the evaluation of the power spectral density was performed over three classes of samples, including $m = 10$, 100 and 300 response histories. The resulting curves are virtually coincident, illustrating the rapid convergence in the calculations, even after averaging the first 10 response histories only. Also, the dashed lines represent results obtained by the linearized model through application of formula (11) and included for comparison purposes. The coincidence of the continuous and dashed curves in Fig. 14 demonstrates that the predictions of the linearized model are sufficiently accurate for the road quality chosen. Moreover, the response of the wheel is much larger than the response of the human components around the frequency range of 10 Hz, where the linearized coupled model presents a mode dominated by the wheel motion. On the other hand, the response of the human components is bigger than the wheel response for excitation with frequency around 1 Hz.

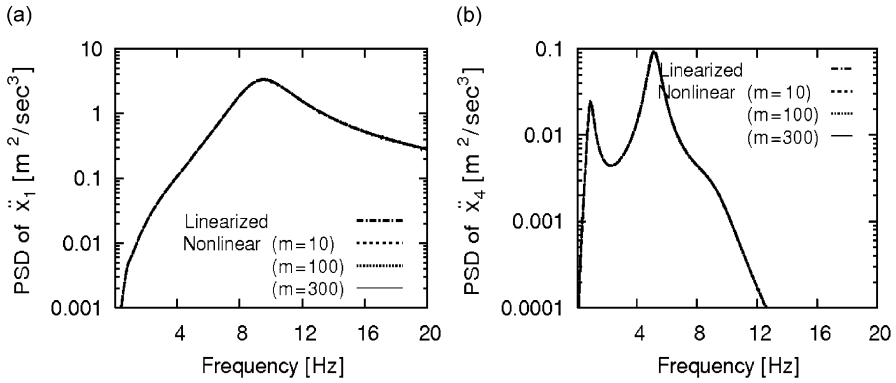

Fig. 14. Power spectral density of the acceleration at: (a) the wheel and (b) the pelvis, caused by class A (very good) quality roads and $v_0 = 120$ km/h.

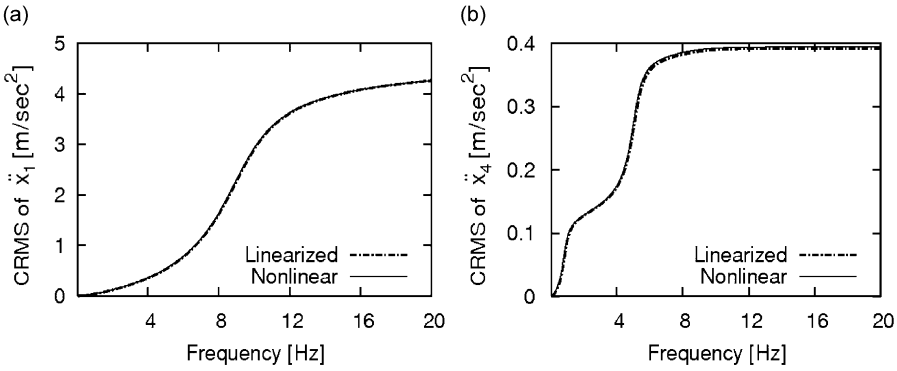

Fig. 15. Cumulative root-mean-square value of the acceleration at: (a) the wheel and (b) the pelvis, caused by class A (very good) quality roads and $v_0 = 120$ km/h.

Successful calculation of the elements of the power spectral density matrix of the response permits the subsequent direct evaluation of other response quantities, like correlation functions, cumulative root-mean-square values, vibration dose and SEAT values, which are useful in assessing the ride comfort of a vehicle [1–4,12]. For instance, Figs. 15a and b present the cumulative root-mean-square value of the acceleration obtained for the wheel and the pelvis, respectively, for the same excitation conditions that led to the results of Fig. 14. These new results indicate that most of the energy in the signals referring to the degrees of freedom of the biodynamic model is distributed in a frequency range below 10 Hz, while a significant potion of the energy in the wheel acceleration signal is concentrated between 10 and 20 Hz.

Similar results were also obtained for class B (good quality) road profiles, with $S_g(\Omega_{\text{ref}}) = 16 \times 10^{-6}\,\text{m}^2/\text{cycle/m}$. At this point, it should be mentioned that the amplitude of the road geometrical profiles belonging to this class is already considerably larger than the amplitudes considered in the harmonic case (Figs. 10 and 12). From this point of view, random excitation seems to be more preferable in experimental studies, since it leads to smaller deviation between the predictions of the nonlinear and the linearized models.

The situation started changing rapidly when road profiles belonging to class C (average quality), with $S_g(\Omega_{\text{ref}}) = 64 \times 10^{-6}\,\text{m}^2/\text{cycle/m}$, were selected. In that case, some combinations of the phases φ_n in formula (12) led to excitation that caused response with excessive amplitudes, which in turn resulted in large deviations of the evaluated statistical quantities from those obtained by the corresponding linearized system. This behavior is expected, since the response of nonlinear systems to stationary random excitation is not necessarily stationary. In order to investigate this phenomenon in more detail, the calculations were repeated after reducing the value of $S_g(\Omega_{\text{ref}})$ to $32 \times 10^{-6}\,\text{m}^2/\text{cycle/m}$, which lies in the border between good and average

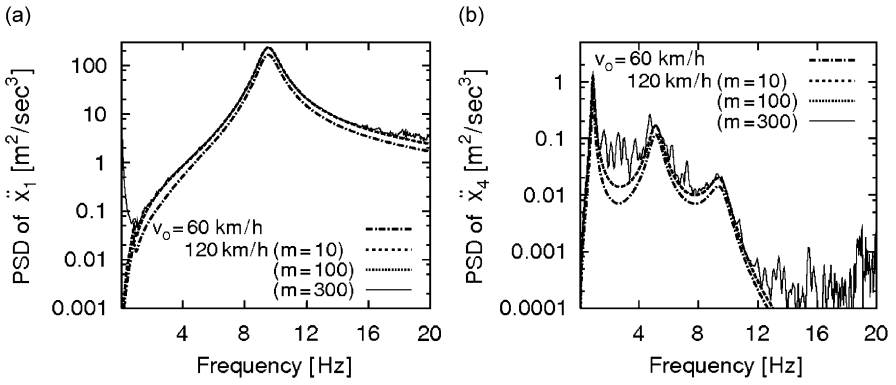

Fig. 16. Power spectral density of the acceleration at: (a) the wheel and (b) the pelvis, caused by class B–C quality roads, for $v_0 = 120$ and $v_0 = 60$ km/h.

quality road groups. The power spectral density determined for the acceleration of the wheel and the pelvis is shown in Figs. 16a and b, respectively. For comparison, the calculations were performed for two horizontal velocities, $v_0 = 60$ and 120 km/h. Clearly, the larger the value of v_0 the larger the value of the power spectral density. More importantly, the predictions of the nonlinear model were found to be very close to the predictions of the corresponding linearized model when $v_0 = 60$ km/h. Likewise, the results determined for $v_0 = 120$ km/m and $m = 10$ or 100 sample histories were also almost coincident with the results obtained by the corresponding linearized model. However, the results obtained by averaging the 300 sample histories started exhibiting a sudden deviation. In fact, it was found that a further increase in the number of samples resulted in even stronger deviation.

In order to explain the situation resulting for the velocity of $v_0 = 120$ km/h, the long time history for the mean square value of the acceleration measured at the wheel was examined. From the results, it became apparent that all the excitation samples selected for $m = 100$ lead to response with comparable amplitudes. However, the response amplitude obtained in one case included in the sample of the 300 motions was much larger than the other motions. In particular, this motion possesses excessive amplitude and was responsible for the deviation observed in the predictions of the linear and nonlinear models observed in Figs. 16a and b for $m = 300$. Namely, when these data were discarded from the averaging, the deviation observed between the predictions of the nonlinear and the corresponding linearized models becomes negligible.

In closing, it is important to note that the appearance of motions with very large amplitude becomes more frequent as the quality of the road group worsens gradually. For instance, it is mentioned that 22 such motions were encountered in the first 300 response samples, obtained for a vehicle traveling with a horizontal speed of $v_0 = 60$ km/h over road profiles belonging to class C, with $S_g(\Omega_{\text{ref}}) = 64 \times 10^{-6}$ m^2/cycle/m. In fact, the appearance of these motions was the main reason for the large deviation observed between the predictions of the nonlinear and the linearized model in that case, as well as for cases with road groups of even worse quality. Once more, these results illustrate that substantial errors arise when someone tries to interpret and use numerical or experimental data obtained from methodologies based on the foundation and using the framework offered by the classical linear vibration theory alone.

4. Synopsis and conclusions

Systematic methodologies were developed for determining response of biodynamic driver-seat lumped parameter models riding on quarter car models. First, the equations of motion of the coupled dynamical system were set up. These equations involved strong nonlinearities due to the action of both the car suspension unit and the components of the human model. They also include the possibility of a temporary loss of contact between the wheel and the ground as well as between the seat and the human pelvis, occurring under certain forcing conditions. The presence of these nonlinearities necessitated the development of appropriate numerical techniques in order to properly integrate the equations of motion and study the dynamic performance of the

vehicle and the passengers under transient, periodic or stationary random road excitation. Then, the influence of certain important parameters of the system was investigated. Among other things, it was shown that consideration of the car model flexibility effects is necessary for improving the accuracy of the coupled model throughout the frequency range of interest. Also, the dynamic quantities determined form a basis for computing other response quantities, like transmissibility functions and root-mean-square values, which are valuable for assessing ride comfort or the possibility of injury due to a shock loading in a vehicle. Moreover, the effect of the nonlinearities was found to become considerable as the amplitude of the excitation increased. Besides leading to large deviations in the response amplitudes predicted by the linearized model, activation of the nonlinearities was shown to be responsible for large amplitude motions and irregular behavior of the dynamical system examined. This introduces a dimension of unpredictability in the response and presents a source of contamination of the measurements, leading to wrong interpretation if it is performed based on linear formulations. Finally, the methodologies presented can be extended to include the effect of other types of excitation or to study more accurate and complicated lumped parameter or finite-element models of both the vehicle and the passengers. Development of more accurate mechanical models will help in a more reliable determination of the dynamic response of the coupled system examined, leading to a reduction in the number of experiments needed in predicting its behavior. Moreover, both the coupled dynamical model and the numerical techniques developed provide a solid basis for future efforts to identify experimentally or to select optimum values of the structural parameters, like the seat technical characteristics.

Acknowledgments

This research was partially supported by a grant from the General Secretariat of Research and Technology, Greek Ministry of Development, through the PENED 2001 program (01-EΔ-330).

References

[1] M.J. Griffin, *Handbook of Human Vibration*, San Diego, Academic Press, 2003.
[2] G.S. Paddan, M.J. Griffin, A review of the transmission of translational seat vibration to the head, *Journal of Sound and Vibration* 215 (1998) 863–882.
[3] M. Kubo, F. Terauchi, H. Aoki, Y. Matsuoka, An investigation into a synthetic vibration model for humans: an investigation into a mechanical vibration human model constructed according to the relations between the physical, phychological and physiological reactions of humans exposed to vibration, *International Journal of Industrial Ergonomics* 27 (2001) 219–232.
[4] S. Wu, S. Rakheja, P.-E. Boileau, Analyses of relationships between biodynamic response functions, *Journal of Sound and Vibration* 226 (1999) 595–606.
[5] P.-E. Boileau, S. Rakheja, S. Wu, A body mass dependent mechanical impedance model for applications in vibration seat testing, *Journal of Sound and Vibration* 253 (2002) 243–264.
[6] N. Yogananden, S. Kumaresan, L. Yoo, A. Pintar, Finite element model of the human lower cervical spine: parametric analysis of the C4-C6, *Journal of Biomechanical Engineering* 119 (1997) 87–92.
[7] S. Kitazaki, M.J. Griffin, A model analysis of whole-body vertical vibration using a finite element model of the human body, *Journal of Sound and Vibration* 200 (1997) 83–103.
[8] C. Papalukopoulos, S. Natsiavas, Driver biodynamics coupled with dynamics of large scale vehicle models. *Third International Conference on Whole-Body Vibration Injuries*, Nancy, France, 2005.
[9] B. Hinz, H. Seidel, The non-linearity of the human body's response during sinusoidal whole body vibration, *Industrial Health* 25 (1987) 169–181.
[10] N.J. Mansfield, M.J. Griffin, Non-linearities in apparent mass and transmissibility during exposure to whole-body vertical vibration, *Journal of Biomechanics* 33 (2000) 933–941.
[11] Z. Zong, K.Y. Lam, Biodynamic response of shipboard sitting subject to ship shock motion, *Journal of Biomechanics* 35 (2002) 35–43.
[12] Y.T. Choi, N.M. Wereley, Mitigation of biodynamic response to vibratory and blast-induced shock loads using magnetorheological seat suspensions. *Proceedings of the IMECE*, Washington, DC, 2003.
[13] International Organization for Standardization, Guide for the evaluation of human exposure to whole body vibration, ISO 2631-1, 1997.
[14] T.D. Gillespie, *Fundamentals of Vehicle Dynamics*, Society of Automotive Engineers, Warrendale, 1992.
[15] D. Karnopp, M.J. Crosby, R.A. Harwood, Vibration control using semi-active generators, *Transactions of the American Society of Mechanical Engineers, Journal of Engineering for Industry* 96 (1974) 619–626.
[16] D. Hrovat, Application of optimal control to advanced automotive suspension design, *Transactions of the American Society of Mechanical Engineers, Journal of Dynamic Systems, Measurement and Control* 115 (1993) 328–342.

[17] G. Verros, S. Natsiavas, C. Papadimitriou, Design optimization of quarter car models with passive and semi-active suspensions under random excitation, *Journal of Vibration and Control* 11 (2005) 581–606.
[18] G. Verros, S. Natsiavas, G. Stepan, Control and dynamics of quarter-car models with dual-rate damping, *Journal of Vibration and Control* 6 (2000) 1045–1063.
[19] R.I. Leine, D.H. van Campen, B.L. van de Vrande, Bifurcations in nonlinear discontinuous systems, *Nonlinear Dynamics* 23 (2000) 105–164.
[20] G. Verros, S. Natsiavas, Dynamics of vehicles with semi-active suspensions exhibiting wheel hop, *Vehicle System Dynamics (supplement)* 35 (2001) 135–148.
[21] Ch. Glocker, *Set-Valued Force Laws—Dynamics of Non-Smooth Systems*, Springer, Berlin, 2001.
[22] J.B. Roberts, P.D. Spanos, *Random Vibration and Statistical Linearization*, Wiley, New York, 1990.
[23] A.H. Nayfeh, B. Balachandran, *Applied Nonlinear Dynamics*, Wiley-Interscience, New York, 1995.
[24] C. Papalukopoulos, S. Natsiavas, Dynamics of large scale mechanical models using multilevel substructuring, *ASME Journal of Computational and Nonlinear Dynamics* 2 (2007) 40–51.
[25] S. Natsiavas, Dynamics of multiple degree of freedom oscillators with colliding components, *Journal of Sound and Vibration* 165 (1993) 439–453.
[26] S.I. Chang, A.K. Bajaj, C.M. Krousgrill, Nonlinear vibrations and chaos in harmonically excited rectangular plates with one-to-one internal resonance, *Nonlinear Dynamics* 4 (1993) 433–460.
[27] D.G. Aronson, M.A. Chory, G.R. Hall, R.P. McGehee, Bifurcations from an invariant circle for two-parameter families of maps of the plane: a computer assisted study, *Communications in Mathematical Physics* 83 (1982) 303–354.
[28] C.J. Dodds, J.D. Robson, The description of road surface roughness, *Journal of Sound and Vibration* 31 (1973) 175–183.